Aerogels

DOI: 10.1002/anie.201410668

Scalable Template Synthesis of Resorcinol–Formaldehyde/Graphene Oxide Composite Aerogels with Tunable Densities and Mechanical Properties**

*Xin Wang, Lei-Lei Lu, Zhi-Long Yu, Xue-Wei Xu, Ya-Rong Zheng, and Shu-Hong Yu**

Abstract: *Resorcinol–formaldehyde (RF) and graphene oxide (GO) aerogels have found a variety of applications owing to their excellent properties and remarkable flexibility. However, the macroscopic and controllable synthesis of their composite gels is still a great challenge. By using GO sheets as template skeletons and metal ions (Co^{2+}, Ni^{2+}, or Ca^{2+}) as catalysts and linkers, the first low-temperature scalable strategy for the synthesis of a new kind of RF–GO composite gel with tunable densities and mechanical properties was developed. The aerogels can tolerate a strain as high as 80% and quickly recover their original morphology after the compression has been released. Owing to their high compressibility, the gels might find applications in various areas, for example, as adsorbents for the removal of dye pollutants and in oil-spill cleanup.*

Aerogels, as highly porous, low-density materials, have recently attracted more and more attention.[1–3] Particularly, 3D interconnected networks with many open pores in the aerogels allow the quick access and diffusion of ions and molecules, which make aerogels suitable as electrode materials for batteries and supercapacitors,[4] elastic conductors,[5] catalyst supports,[6] and for the treatment of polluted water.[7] Resorcinol formaldehyde (RF) aerogels, as a kind of traditional organic aerogels, were first obtained by Pekala and coworkers through the aqueous polycondensation of resorcinol with formaldehyde.[8] These RF aerogels are inexpensive, they feature a low thermal conductivity and high porosity and have found applications in various areas, for example, as thermal insulators and precursors to functional carbon aerogels.[9–12] However, the practical application of traditional RF aerogels is hindered by the limitations of industrial supercritical-drying techniques and poor mechanical properties, as these aerogels are usually brittle and fragile.[13,14] Therefore, methods to obtain flexible RF-based aerogels with a more simple drying method (such as freeze drying) are very important for boosting its application.

Graphene oxide (GO), owing to its excellent dispersion in water and abundant surface functional groups, is a promising building block for 3D architectures, such as films, monoliths, gels, and graphene/polymer composites, which can be subsequently pyrolyzed to various carbon materials of use in energy-related applications.[15–20] In particular, highly compressible monoliths that are solely based on GO sheets have been successfully fabricated in recent years, which confirmed the great potential of GO as a skeleton for synthesizing compressible 3D materials.[21] Furthermore, some metal ions (such as Co^{2+}, Ni^{2+}) can act as cross-linkers for assembling GO into 3D porous gels and substitute the traditional catalysts (Na_2CO_3) used for the polymerization of resorcinol/formaldehyde (RF).[22,23] Thus, the incorporation of flexible GO within a RF material is a possible method to improve the brittleness of a simple RF aerogel, which would be beneficial to extend its applicability.

Although there have been several reports on RF–GO monoliths, the obtained products were still brittle, incompressible, and had a high density.[24,25] Recently, a family of phenolic resin gels was synthesized by using chitosan networks as templates.[26] Herein, using GO sheets as template skeletons and metal ions (Co^{2+}, Ni^{2+}, or Ca^{2+}) as catalysts and linkers, we developed a low-temperature route to synthesize a new type of RF–GO–metal compressible aerogel. This method can be easily scaled up from 25 mL to 500 mL just by using a larger autoclave. Compared to traditional fragile and brittle RF aerogels, in our synthesis process, the synergistic effects of GO and the metal ions improve the mechanical behavior of the as-prepared RF-based aerogels. In particular, the metal ions play two important roles: 1) They induce the formation of GO and RF 3D networks by coordination. 2) They adjusting the pH value of the solution by acting as acid catalysts to control the degree of cross-linking between resorcinol and formaldehyde. Owing to their excellent compressibility and high chemical reactivity, the RF–GO–metal aerogels can be applied as solid adsorbents for the removal of dye pollutants.

Photographs of the reaction solution and the thus obtained gel products are shown in Figure 1a. Resorcinol, formaldehyde, and the metal salt ($CoCl_2 \cdot 6H_2O$) were first dissolved in a GO dispersion to form a homogenous mixture. Then, heating the solution at 85 °C for 24 hours resulted in

[*] Dr. X. Wang, L. L. Lu, Dr. Z. L. Yu, Dr. X. W. Xu, Dr. Y. R. Zheng, Prof. Dr. S. H. Yu
Division of Nanomaterials & Chemistry
Hefei National Laboratory for Physical Sciences at Microscale
Collaborative Innovation Center of Suzhou Nano Science and Technology, CAS Key Laboratory of Mechanical Behavior and Design of Materials, Department of Chemistry, University of Science and Technology of China
Hefei, Anhui 230026 (P. R. China)
E-mail: shyu@ustc.edu.cn
Homepage: http://staff.ustc.edu.cn/~yulab/

[**] This work is supported by the Ministry of Science and Technology of China, the National Basic Research Program of China (2014CB931800, 2010CB934700, 2013CB933900), the National Natural Science Foundation of China (21431006, 91022032, 91227103, 2060190175), and the Chinese Academy of Sciences (KJZD-EW-M01-1).

Supporting information for this article is available on the WWW under http://dx.doi.org/10.1002/anie.201410668.

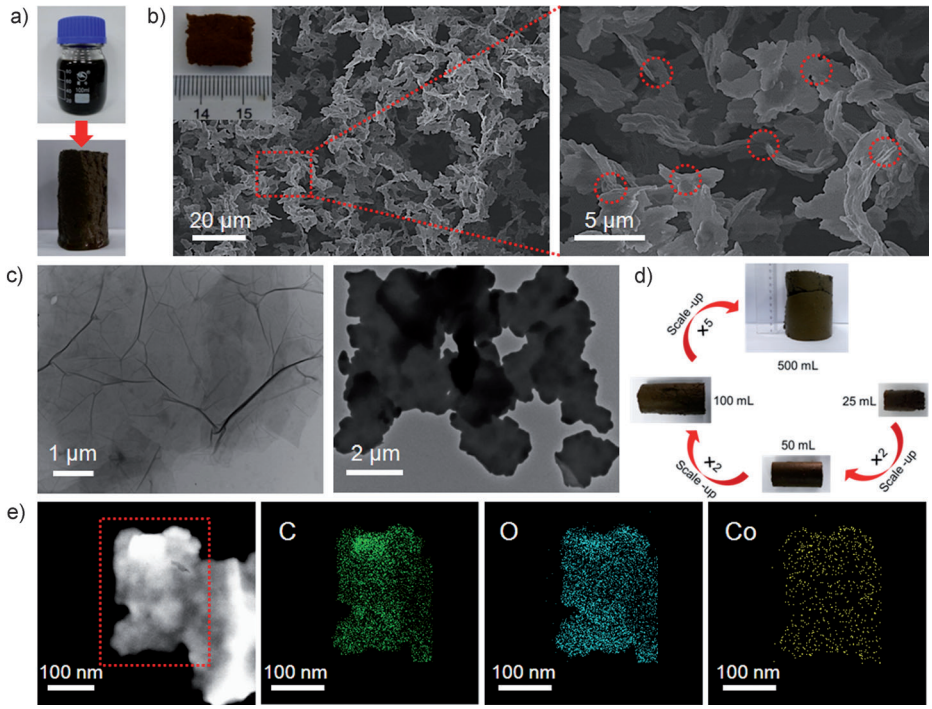

Figure 1. Large-scale synthesis and characterization of the RF–GO–Co aerogels. a) Photographs of the reaction solution and the resulting gel. b) SEM images of the RF–GO–Co composite aerogel with different magnifications. Inset: a photograph of the RF–GO aerogel obtained after cutting and freeze drying. The red circles represent the junctions between sheets. c) TEM images of sheets before and after the hydrothermal treatment. Left: free-standing GO; right: final product of composite sheets. d) Scale-up of the synthesis of the RF–GO gels. e) TEM image and EDX elemental mappings of C, O, and Co.

a well-defined, brown, gel-like product, which occupied the whole space of the Teflon container with a columnar shape and could be taken out directly. The obtained wet gels could be easily cut into any desired shape with a sharp blade. After washing with water to remove any residues, the as-prepared hydrogels were freeze-dried to form RF–GO–metal composite aerogels. The scanning electron microscopy (SEM) images of the aerogels in Figure 1b demonstrate that a well-organized highly porous 3D network microstructure consisting of 2D sheets has been formed. These sheets with a thickness of approximately 300 nm are highly interconnected with each other through a great number of junctions, which is probably responsible for the good mechanical properties of the aerogel. Transmission electron microscopy (TEM) images show the microstructure of the sheets before and after the reaction (Figure 1c). The left image reveals the features of free-standing GO. After hydrothermal treatment, pure GO flakes are indistinguishable, and the sheets become very thick, which indicates that the GO sheets might be covered with RF layers.

One of the advantages of our method is its scalability. As shown in Figure 1d, the preparation of the RF–GO–Co gels can be easily scaled up from 25 mL to 500 mL just by using a larger autoclave and without changing the reactant concentrations or the reaction time. A further scale-up for industrial production should also be possible with an even larger reaction vessel. The elemental mapping in Figure 1e confirms the homogeneous distributions of C, O, and Co in the aerogel sheets. To investigate the fate of the Co^{2+} ions in the final aerogels, X-ray photoelectron spectroscopy (XPS) was used to study the chemical state of Co in the products (Figure S1). It was found that Co was present in the final composite aerogels and maintained its original valence of +2. The main peak at 781.3 eV can be ascribed to oxygen-coordinated Co^{2+}, which is shifted towards a higher binding energy (BE) by approximately 1 eV compared with common Co–O motifs.[27] This variation may be related to the fact that the Co^{2+} ion is tetrahedrally coordinated by O atoms, reducing the electron density on the cobalt. Moreover, the signal at 783.4 eV is associated with excessive Co ions, and the other two peaks at higher BE correspond to satellites.[28]

Owing to the versatility of the synthesis, the apparent density and compressibility of the aerogels can be varied by changing the synthetic parameters (Supporting Information, Table S1 and Figure S2–S6). The RF–GO–Co aerogels display great compressibility only when the amount of $CoCl_2{\cdot}6H_2O$ is at an appropriate value (0.1–0.2 g per 20 mL). This demonstrates that Co^{2+} acts as a catalyst regulating the pH value of the solution to improve the polymerization rate of RF, which results in the specific 3D structure and excellent mechanical properties. Compared with traditional RF aerogels, all of the composite aerogels are very light. The density of the lightest RF–GO–Co aerogel that we have prepared is only 15.7 mg cm^{-3}, which can possibly be pyrolyzed into an ultralight carbon aerogel with potential applications for oil-spill cleanup. Furthermore, the freeze-drying process is also important for the properties of the compressible RF–GO–Co aerogel. When the hydrogel was dried at 60 °C in an oven, the product aerogel lost its compressibility and became hard (Figure S7). This is attributed to further polymerization of RF at 60 °C, which was confirmed by the increase in density of the RF–GO–Co aerogel (31.2 to 72.4 mg cm^{-3}; Table S1).

Among all of the synthesized aerogels listed in Table S1, the composite aerogel RF–GO–Co 3 displays the best compressibility, and it could stand large deformations without any damage. Compared to common, brittle RF- and silica-based aerogels,[25,29] the RF–GO–Co 3 aerogel can tolerate a high compression strain. In Figure 2a, it is illustrated that a compressible RF–GO–Co aerogel completely recovered its original shape without any mechanical fracture after the external compression had been removed. Compressive stress–strain curves for the compressible RF–GO–Co aerogel at maximum strains (ε) of 30, 50, and 80% are shown in Figure 2b. Two

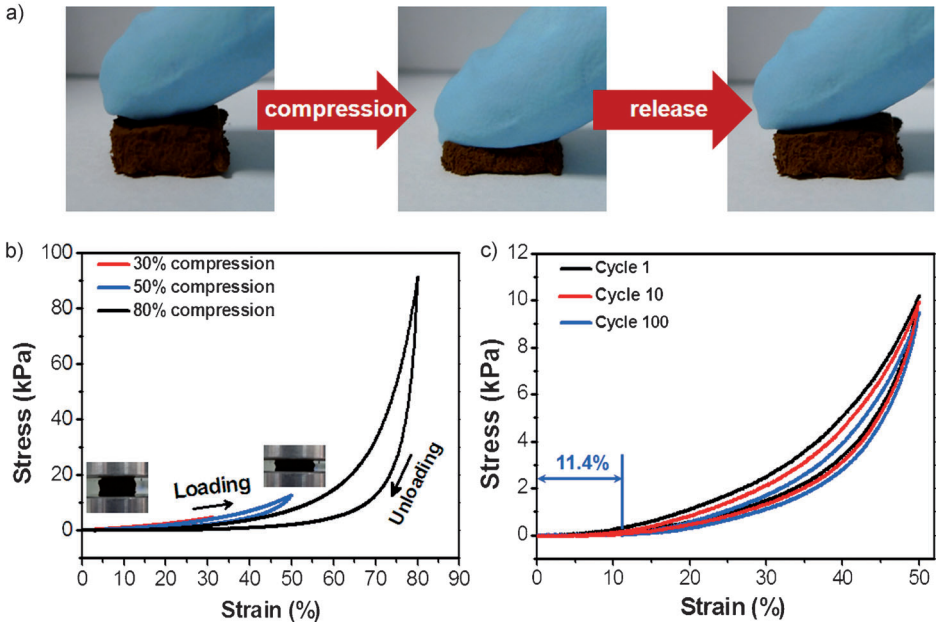

Figure 2. Mechanical performance of the compressible RF–GO–Co composite aerogel. a) Photographs showing that the RF–GO–Co aerogel can recover its original shape after a strong compression. b) Compressive stress–strain curves of the RF–GO–Co aerogel at different set strains of 30, 50, and 80%. Inset: Sequential photographs of the RF–GO–Co aerogel during the compression process. c) Cyclic stress–strain curves of the RF–GO–Co aerogel at a maximum strain of 50%, showing a permanent plastic deformation of 11.4% after 100 cycles.

distinct regions were observed during the loading process, namely a linear elastic region at $\varepsilon < 60\%$ and a densification region at $\varepsilon > 60\%$. In the linear elastic region, the aerogel gradually shrinks, and the compressive stress slowly increases with the strain, which results from the elastic bending of the interconnected sheet structures. In the densification region at $\varepsilon > 60\%$, the aerogel is conformably densified, and the stress increases steeply with compression owing to the continuous reduction in the pore volume. Furthermore, during the unloading process, the stress remains above zero until $\varepsilon = 0$, indicating that the aerogels can rapidly and fully recover their original morphology, which is a very important property for energy absorption materials. The maximum stress (at $\varepsilon = 50\%$) of the aerogel is approximately 12.7 kPa, which indicates that our synthesized RF–GO–Co aerogel is a relatively soft material. Dynamic viscoelastic measurements further describe the structure and properties of the compressible RF–GO–Co aerogel (Figure S8). As a function of angular frequency (1–60 rad/s), the storage modulus is one order of magnitude higher than the loss modulus, indicating that the elastic response is predominant in the 3D cross-linked network of the aerogel (Figure S8a). Furthermore, the aerogel also has a good thermal stability as demonstrated by independent storage and the loss modulus for a temperature range (25–95 °C; Figure S8b).

The fatigue strain–stress curves at $\varepsilon = 50\%$ with 100 loading/unloading cycles are shown in Figure 2c. The maximum degradation under compressive stress is smaller than 10% after 100 cycles, and the plastic deformation only amounts to approximately 11.4% after fatigue testing, which corroborates the excellent structural robustness of the compressible RF–GO–Co aerogel. No obvious structural changes were observed after the cycling tests (Figure S9). In comparison, the plastic deformation for polymeric foams at $\varepsilon \approx 20\%$ is typically 10–30%, and nanotube-based foams usually have a plastic deformation of 8–20% with degradation under a compressive stress of 20–30% at similar strain. Importantly, aside from Co^{2+}, other metal ions, such as Ni^{2+} or Ca^{2+}, can also induce the formation of compressible RF–GO–metal aerogels with similar microstructures (Figure S10). Based on the above results, in combination with previous reports on compressible aerogels, we have developed the first synthesis of highly compressible RF-based aerogels, and their mechanical properties are also comparable to those of several other relevant compressible aerogels (Table S2). For example, traditional RF aerogels with an apparent density of $< 100\ mg\,cm^{-3}$ are brittle and have a maximum strain of only 9%.[30] Other common flexible aerogels, such as graphene aerogels[21,31] and nanocellulose-based aerogels,[32–34] feature a better compressibility (as high as 90%), but their shape recovery after a large strain is worse than for our RF–GO–metal aerogels. The improved overall mechanical properties, including high compressibility, rapid shape recovery, and good cycling stability, render our gels more suitable as solid compressible adsorbents for the removal of dye pollutants.

To understand the possible interactions between the GO sheets and the RF species in the aerogels and to further elucidate the role of Co^{2+} in the formation process, a series of experiments were carried out (Figure S11–S13). Without addition of GO or RF, we could not obtain a gel-like product after heating at 85 °C for 24 hours (Figure S11a). Comparing the X-ray diffraction (XRD) patterns of the RF–GO–Co aerogels and of GO materials that were obtained by a hydrothermal process at 85 °C, we found that the characteristic diffraction peaks of GO disappeared after the reaction. This indicates that the GO sheets are possibly coated with an amorphous polymer layer (RF; Figure S11b). Furthermore, we analyzed the FTIR spectra of GO, RF, and the RF–GO–Co aerogels (Figure S11c). After heating at 85 °C for 24 hours, the peaks of pure GO became weaker, indicating that GO was partly reduced. The spectrum of the RF–GO–Co aerogel exhibits obvious peaks at 3000–3500, 2925, 2853, 1614, 1479, 1219, and 1090 cm^{-1}, which correspond to O–H stretching, CH_2 stretching, aromatic ring stretching, CH_2 bending vibrations, and the asymmetric and symmetric stretching of methylene ether (CH–O–CH) and thus to the IR spectrum of

RF.[25,35] The IR spectra thus confirm that polymerization of RF has occurred during the fabrication process.

To further understand the formation process of such aerogels, we conducted a set of experiments on the effect of the reaction time (Figure S12). As shown in the SEM and TEM images, at the initial stage (2 h), typical flake-like shapes of GO can be clearly observed. With prolonged reaction times (4 or 8 h), the thickness of the sheets gradually increased, and the characteristic edges of the GO sheets became poorly defined. After 12 h, these thick sheets were linked together to form a 3D structure, and pure GO flakes were indistinguishable in the TEM image, which confirms that GO indeed acts as a template skeleton to be covered in RF during the formation of the RF–GO–Co aerogels. In addition, to confirm the particular role of Co^{2+} for the great compressibility of these aerogels, two kinds of RF–GO aerogels were synthesized: a RF–GO aerogel without Co^{2+} and a similar aerogel for which the pH value of the solution was pre-adjusted to 3.1 with HCl before the hydrothermal process (the same pH value as that obtained with 0.2 g of $CoCl_2{\cdot}6H_2O$; Figure S13). It was found that independent of the pH value of the initial reaction solution, the resulting aerogels without Co^{2+} always had 3D structures consisting of thin sheets and were brittle. According to previous reports, divalent metal ions can link GO to polymers through coordination, and the oxygen atoms in RF can also be coordinated to transition-metal cations when metal salts are used as the polymerization catalysts.[36,37] Hence, we speculate that in our RF–GO–Co aerogels, Co^{2+} is bound to oxygen-containing functional groups of GO and RF through coordination, which leads to improved mechanical properties. To confirm this hypothesis, we examined the coordination environment of the Co^{2+} ions in the aerogels by electron spin resonance (ESR) spectroscopy (Figure S14). As shown in the ESR spectra recorded at different temperatures (2, 10, 50 K), the large signal at $g = 5.1$ corresponds to a high-spin Co^{2+} ion with tetrahedral coordination.[38] Generally, high-spin Co^{2+} complexes are obtained with weak-field ligands. In our case, only the oxygen-containing groups in RF and GO can act as such ligands. Therefore, we can conclude that the Co^{2+} ions are found in a four-coordinate environment (Co–O) within our compressible aerogels.

Based on the above analysis, we have developed a structural model for the novel compressible RF–GO–metal aerogel, which is depicted in Scheme 1. In the aerogel, three types of bonding interactions exist, which result in the 3D network structure and the high compressibility: 1) Metal ions link the RF and GO networks; 2) the cross-linked RF structure is obtained by the formation of covalent bonds, and 3) hydrogen bonds link RF and GO. During the synthesis process, the GO sheets are interconnected by metal ions through coordination.[23] Simultaneously, metal ions also link GO sheets with chemically linked RF by coordination between the hydroxy groups of RF and the oxygen-containing groups in GO. Aside from the interactions induced by the metal ions, hydrogen bonds also contribute to the strong linkage between RF and GO. As the reaction proceeds, RF finally polymerized to a specific degree under the acidic conditions regulated by the metal ions, which also contributes to the high compressibility of the aerogel.[37] Thus, an integrated, stable, and compressible RF–GO–metal aerogel can be obtained.

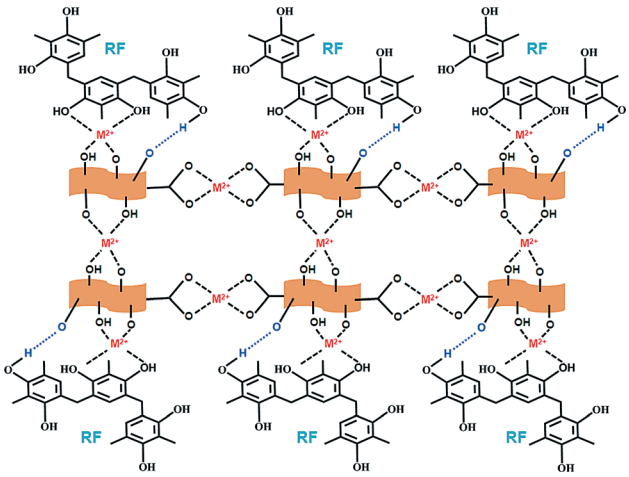

Scheme 1. Structural model of the RF–GO–metal aerogels.

Resins and GO-based materials, which feature a large number of oxygen-containing groups, are often used as adsorbents for ionic pollutants.[39,40] Therefore, given the excellent flexibility, high porosity, and the high number of oxygen-containing groups, the as-prepared RF–GO–Co gels can be used directly as compressible adsorbents for the facile removal of dye pollutants. The overall process is shown in Figure 3. A RF–GO–Co hydrogel was first strongly compressed ($\varepsilon > 50\,\%$) to squeeze out most of the water inside and then immerged in a methylene blue (MB) solution ($10\ mg\,L^{-1}$). After one minute, the hydrogel was saturated with MB solution and almost recovered its initial shape without any fracture. Then, the saturated hydrogel was taken out and compressed again to squeeze out the purified water, which appeared to be greatly decolorized and clear compared with the original MB solution. According to UV/Vis spectroscopic analysis of the decontaminated water after adsorption, the removal percentage of MB is as high as 97.9 %. Furthermore, the adsorption process is easily repeated without a special treatment of the hydrogel; even after 20 adsorption cycles, the RF–GO–Co compressible gel could still maintain an adsorption capacity of 87 % for the MB solution.

In conclusion, we have fabricated a new kind of compressible RF–GO–metal aerogel through a low-temperature process by using GO sheets as template skeletons and metal ions (Co^{2+}, Ni^{2+}, or Ca^{2+}) as catalysts and linkers. The versatility of this method allows for its simple scale-up from 25 mL to 500 mL. Unlike traditional, fragile and brittle RF aerogels, the synthesized RF–GO–metal composite aerogels exhibit an excellent compressibility, which can tolerate a strain as high as 80 %. Owing to the enhanced mechanical properties, the applicability of RF-based aerogels will be extended, for example, they could be used as solid adsorbents for the removal of dye pollutants.

Received: November 2, 2014
Revised: December 2, 2014
Published online: January 12, 2015

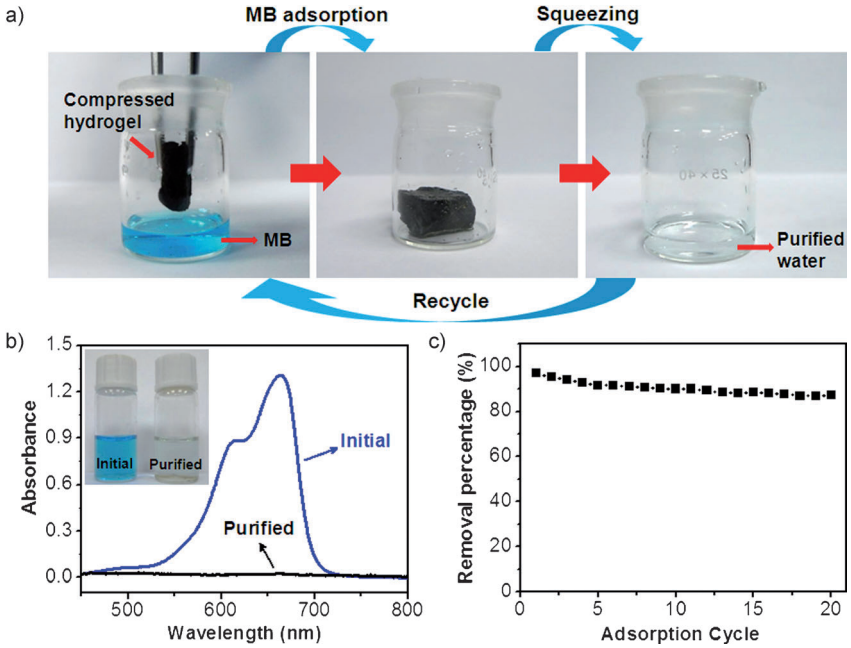

Figure 3. Adsorption properties of the compressible RF–GO–Co composite hydrogels for a dye pollutant (MB). a) Photographs illustrating the facile removal of MB by using the excellent adsorption abilities and compressibility of the hydrogel. b) Absorption spectra of the initial MB solution (10 mg L^{-1}) and the purified solution after the first uptake–squeezing process. Inset: Photographs of the corresponding solutions. c) Removal percentage of MB as a function of the number of adsorption cycles.

Keywords: aerogels · compressibility · graphene oxide · resorcinol

[1] N. Hüsing, U. Schubert, *Angew. Chem. Int. Ed.* **1998**, *37*, 22–45; *Angew. Chem.* **1998**, *110*, 22–47.
[2] A. C. Pierre, G. M. Pajonk, *Chem. Rev.* **2002**, *102*, 4243–4266.
[3] T. A. Schaedler, A. J. Jacobsen, A. Torrents, A. E. Sorensen, J. Lian, J. R. Greer, L. Valdevit, W. B. Carter, *Science* **2011**, *334*, 962–965.
[4] Y. Zhao, J. Liu, Y. Hu, H. Cheng, C. Hu, C. Jiang, L. Jiang, A. Cao, L. Qu, *Adv. Mater.* **2013**, *25*, 591–595.
[5] J. Ge, H.-B. Yao, X. Wang, Y.-D. Ye, J.-L. Wang, Z.-Y. Wu, J.-W. Liu, F.-J. Fan, H.-L. Gao, C.-L. Zhang, S.-H. Yu, *Angew. Chem. Int. Ed.* **2013**, *52*, 1654–1659; *Angew. Chem.* **2013**, *125*, 1698–1703.
[6] Z.-S. Wu, S. Yang, Y. Sun, K. Parvez, X. Feng, K. Müllen, *J. Am. Chem. Soc.* **2012**, *134*, 9082–9085.
[7] G. Hayase, K. Kanamori, M. Fukuchi, H. Kaji, K. Nakanishi, *Angew. Chem. Int. Ed.* **2013**, *52*, 1986–1989; *Angew. Chem.* **2013**, *125*, 2040–2043.
[8] R. W. Pekala, *J. Mater. Sci.* **1989**, *24*, 3221–3227.
[9] X. Lu, M. C. Arduini-Schuster, J. Kuhn, O. Nilsson, J. Fricke, R. W. Pekala, *Science* **1992**, *255*, 971–972.
[10] J. Biener, M. Stadermann, M. Suss, M. A. Worsley, M. M. Biener, K. A. Rose, T. F. Baumann, *Energy Environ. Sci.* **2011**, *4*, 656–667.
[11] G. P. Hao, W. C. Li, D. Qian, G. H. Wang, W. P. Zhang, T. Zhang, A. Q. Wang, F. Schüth, H. J. Bongard, A. H. Lu, *J. Am. Chem. Soc.* **2011**, *133*, 11378–11388.
[12] J. Liu, T. Yang, D.-W. Wang, G. Q. Lu, D. Zhao, S. Z. Qiao, *Nat. Commun.* **2013**, *4*, 2798.
[13] A. M. Elkhatat, S. A. Al-Muhtaseb, *Adv. Mater.* **2011**, *23*, 2887–2903.
[14] M. Schwan, L. Ratke, *J. Mater. Chem. A* **2013**, *1*, 13462.
[15] S. H. Lee, H. W. Kim, J. O. Hwang, W. J. Lee, J. Kwon, C. W. Bielawski, R. S. Ruoff, S. O. Kim, *Angew. Chem. Int. Ed.* **2010**, *49*, 10084–10088; *Angew. Chem.* **2010**, *122*, 10282–10286.
[16] Z. Tang, S. Shen, J. Zhuang, X. Wang, *Angew. Chem. Int. Ed.* **2010**, *49*, 4603–4607; *Angew. Chem.* **2010**, *122*, 4707–4711.
[17] W. Wan, L. Li, Z. Zhao, H. Hu, X. Hao, D. A. Winkler, L. Xi, T. C. Hughes, J. Qiu, *Adv. Funct. Mater.* **2014**, *24*, 4915–4921.
[18] S. Chen, J. Duan, M. Jaroniec, S. Z. Qiao, *Angew. Chem. Int. Ed.* **2013**, *52*, 13567–13570; *Angew. Chem.* **2013**, *125*, 13812–13815.
[19] Y. Jiao, Y. Zheng, M. Jaroniec, S. Z. Qiao, *J. Am. Chem. Soc.* **2014**, *136*, 4394–4403.
[20] Y. Zheng, Y. Jiao, Y. Zhu, L. H. Li, Y. Han, Y. Chen, A. Du, M. Jaroniec, S. Z. Qiao, *Nat. Commun.* **2014**, *5*, 3783.
[21] H. Hu, Z. Zhao, W. Wan, Y. Gogotsi, J. Qiu, *Adv. Mater.* **2013**, *25*, 2219–2223.
[22] T. F. Baumann, G. A. Fox, J. H. Satcher, N. Yoshizawa, R. Fu, M. S. Dresselhaus, *Langmuir* **2002**, *18*, 7073–7076.
[23] X. Jiang, Y. Ma, J. Li, Q. Fan, W. Huang, *J. Phys. Chem. C* **2010**, *114*, 22462–22465.
[24] M. A. Worsley, P. J. Pauzauskie, T. Y. Olson, J. Biener, J. H. Satcher, T. F. Baumann, *J. Am. Chem. Soc.* **2010**, *132*, 14067–14069.
[25] G. Wei, Y.-E. Miao, C. Zhang, Z. Yang, Z. Liu, W. W. Tjiu, T. Liu, *ACS Appl. Mater. Interfaces* **2013**, *5*, 7584–7591.
[26] Z.-L. Yu, Z.-Y. Wu, S. Xin, C. Qiao, Z.-Y. Yu, H.-P. Cong, S.-H. Yu, *Chem. Mater.* **2014**, DOI: 10.1021cm504036u.
[27] J. Tang, T. Wang, X. Pan, X. Sun, X. Fan, Y. Guo, H. Xue, J. He, *J. Phys. Chem. C* **2013**, *117*, 16896–16906.
[28] Q. Liu, J. Zhang, *Langmuir* **2013**, *29*, 3821–3828.
[29] A. Fidalgo, M. E. Rosa, L. M. Ilharco, *Chem. Mater.* **2003**, *15*, 2186–2192.
[30] R. W. Pekala, C. T. Alviso, J. D. LeMay, *J. Non-Cryst. Solids* **1990**, *125*, 67–75.
[31] Y. Li, J. Chen, L. Huang, C. Li, J.-D. Hong, G. Shi, *Adv. Mater.* **2014**, *26*, 4789–4793.
[32] F. Jiang, Y.-L. Hsieh, *J. Mater. Chem. A* **2014**, *2*, 350–359.
[33] M. Wang, I. V. Anoshkin, A. G. Nasibulin, J. T. Korhonen, J. Seitsonen, J. Pere, E. I. Kauppinen, R. H. A. Ras, O. Ikkala, *Adv. Mater.* **2013**, *25*, 2428–2432.
[34] H. Sehaqui, M. Salajkova, Q. Zhou, L. A. Berglund, *Soft Matter* **2010**, *6*, 1824–1832.
[35] S. Mulik, C. Sotiriou-Leventis, N. Leventis, *Chem. Mater.* **2007**, *19*, 6138–6144.
[36] H.-P. Cong, P. Wang, S.-H. Yu, *Small* **2014**, *10*, 448–453.
[37] C. Moreno-Castilla, F. J. Maldonado-Hódar, A. F. Pérez-Cadenas, *Langmuir* **2003**, *19*, 5650–5655.
[38] E.-M. El-Malki, D. Werst, P. E. Doan, W. M. H. Sachtler, *J. Phys. Chem. B* **2000**, *104*, 5924–5931.
[39] V. Chandra, J. Park, Y. Chun, J. W. Lee, I.-C. Hwang, K. S. Kim, *ACS Nano* **2010**, *4*, 3979–3986.
[40] A. S. Knight, E. Y. Zhou, J. G. Pelton, M. B. Francis, *J. Am. Chem. Soc.* **2013**, *135*, 17488–17493.